

Analysis of a Building Power System with a Rooftop PV Array and PHEVs as an Aggregator

Young-Jin Kim, James L. Kirtley Jr.

Dept. of Electrical Engineering and Computer Science
Massachusetts Institute of Technology
Cambridge, Massachusetts, USA
powersys@mit.edu, kirtley@mit.edu

Leslie K. Norford

Dept. of Architecture
Massachusetts Institute of Technology
Cambridge, Massachusetts, USA
lnorford@mit.edu

Abstract— As the penetration of photovoltaic (PV) systems on building rooftops increases, the accumulated effects of the rooftop PV output fluctuation on the electric utility are no longer negligible. Energy storage systems have been used to smooth PV power, especially when the building load becomes low. Commercial buildings are increasingly expected to charge or discharge plug-in hybrid electric vehicles (PHEVs), which can be regarded as distributed energy storage. This paper presents an alternative power system for commercial buildings, which compensates for rooftop PV power fluctuation by charging or discharging PHEV batteries, and moreover, participates in tracking frequency regulation signals. The proposed system is designed and implemented using steady-state and dynamic models of power converters and controllers. Simulation studies performed in MATLAB/SIMULINK verify that the objective can be achieved under various conditions, determined by such factors as the maximum voltage, minimum state-of-charge, and desired PHEV charging end-time.

Index Terms-- commercial buildings, frequency regulation, maximum voltage, minimum state-of-charge, plug-in hybrid electric vehicles, rooftop photovoltaic systems.

I. INTRODUCTION

A number of small and medium-sized photovoltaic (PV) generators have been recently installed on the rooftops of residential or commercial buildings, and provide fluctuating power to electric networks especially when the building load becomes low. Therefore, the accumulated output power of the rooftop PV generators in distribution power systems is no longer negligible [1], [2]. In addition, system operators have devised regulations that require distributed generators (DGs) to participate in grid frequency control, and have applied these regulations not only to DGs owned by utility companies, but also to those belonging to independent power producers (IPPs) [3], [4]. As a result, the maximum capacity of the PV system is sometimes limited by the minimum building load, or batteries are considered to cope with the excess PV power [5], [6].

Continuing load growth, unless matched with growth in generation, will result in a stressed and less secure power system operation, and the situation is expected to be aggravated by an increase in electricity demand for electric

vehicles (EVs) and plug-in hybrid EVs (PHEVs). However, with proper system implementation, the PHEVs are envisioned to not only feed energy back into the grid but also provide frequency regulation ancillary service [7]. Batteries have fast dynamic response suitable for high frequency and high power cycling operation, and PHEV battery lifetime degradation is mainly affected by deep depth of discharge encountered while driving, rather than small swings of state of charge (SOC) [8], [9]. Therefore, using PHEVs in a cost-effective way for the compensation for intermittent renewable generator output or load variation has been widely studied [7], [10].

Based on the average short driving distance of a vehicle, it is predicted that most PHEVs are parked and plugged into the grid through building power systems. Therefore, the buildings become important aggregators under the control of a central load dispatching center or local control centers [10]. In regard to the aggregator system configuration, [6] shows that DC-DC converters have higher efficiency than AC-DC inverters, which makes a strong argument for investigating the benefits of directly coupling DC power sources (PV generators) with DC loads (PHEVs) in buildings. In Table I, the energy density comparison implies that PHEVs can be significantly recharged for commuting by PV arrays, which supports the applications of PV system to PHEV charging.

TABLE I. ENERGY DENSITY COMPARISON OF PV AND PHEV [10]–[14]

PV	<ol style="list-style-type: none">1. Typical insolation in the US: 4 kWh/m²/day ~ 6.5 kWh/m²/day2. Average efficiency of commercial solar panels: 10 % (typical) ~ 20 % (high-end)3. General efficiency of DC/DC converter: 95 % ▶ PV output energy density per unit area: 0.475 kWh/m²/day
PHEV	<ol style="list-style-type: none">1. PHEV battery capacity: from 8 kWh to 28 kWh2. Average area for one vehicle: 16.8 m² (25 ~ 30 m² if aisle and circulation areas are included) ▶ PHEV battery energy density per unit area: 0.542 kWh/m² (with assuming initial SOC = 20 %)

Based on these observations, this paper presents an alternative system configuration for a commercial building with a rooftop PV generator and multiple PHEVs in its parking lot. The proposed building system enables the rooftop PV array power fluctuation to be hidden from utility operators.

Furthermore, each PHEV is capable of being charged or discharged with a different amount of power under various conditions, determined by such factors as initial SOC level and the limitations of maximum battery voltage and minimum SOC. Finally, at the same time, the building can actively participate in frequency regulation. For physical analysis in time scales of seconds, the proposed system is designed and implemented with averaged circuit dynamic or steady-state models of power electronic devices and controllers. Simulation studies performed in MATLAB/SIMULINK demonstrate the proper operation of the proposed system.

II. BUILDING POWER SYSTEM DESCRIPTION

A. AC-DC Bidirectional Inverter

Fig. 1 presents an averaged circuit dynamic model of the AC-DC inverter and its duty ratio controller [15]. The inverter not only rectifies the AC power for the PHEV battery charging, but also converts the DC power coming from the rooftop PV array and batteries in a vehicle-to-grid (V2G) mode.

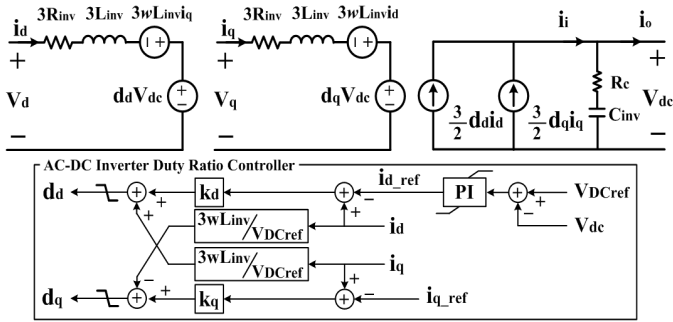


Fig. 1. Average model of an AC-DC inverter and its duty ratio controller

The dq -axis voltages v_d and v_q are calculated using a phase-locked loop (PLL) with the input power, total line impedance, and line voltage at points of common coupling (PCCs). In the control diagram, the term $3wL_{inv}/V_{DCref}$ is added to reduce the cross-coupling between the dq -axis currents i_d and i_q so that they are independently controlled to regulate the DC link voltage V_{dc} and reactive power, respectively. This paper considers the building system operating with unity power factor. Furthermore, the AC grid is simply assumed to have balanced line voltage and impedance.

B. Rooftop PV generator and DC-DC Boost Converter

The rooftop PV array is modeled as a parallel connection of series-wired PV modules, which can be represented as a current source model, as shown in Fig. 2.

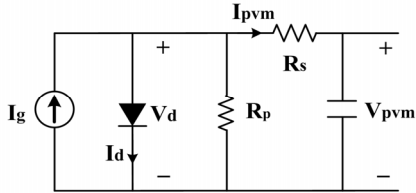


Fig. 2. Equivalent circuit model of a PV module

The nonlinear $I_{pvm}-V_{pvm}$ characteristics equations of the PV module are presented in many studies [16], [17]. The PV array is then connected in parallel to the common DC link through the DC-DC boost converter implemented using the steady-

state model, in which power conversion loss is considered. The power loss may result from internal resistance in passive elements and device switching. In addition, to maximize the PV output power by tracking the maximum power point (MPP), the converter duty ratio is controlled by the incremental conductance method.

C. PHEV Batteries and DC-DC Buckboost Converter

In this paper, the PHEV batteries compensate for the rooftop PV output fluctuation and the rapidly varying component of the frequency regulation signal. There are several battery models with similar characteristics [17]–[19]. In particular, [19] applies a voltage source model, shown in Fig. 3, which is nonlinearly controlled by (1) and (2). The model simplifies parameter extraction from the manufacturer datasheet as well as voltage and SOC calculation under time-varying charging or discharging current.

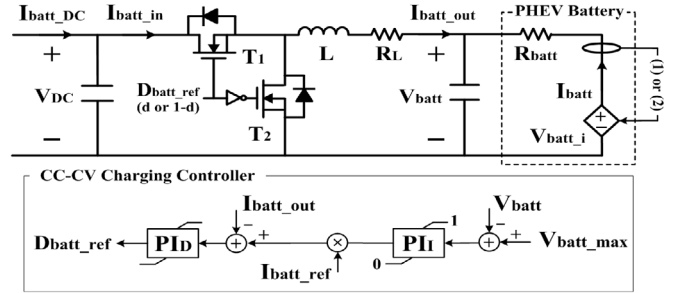


Fig. 3. PHEV battery connected to DC link through a DC-DC converter

a) Discharging ($I_{batt} \geq 0$)

$$V_{batt_i} = V_0 - k \frac{Q \cdot it}{Q - it} - k \frac{Q}{Q - it} I_{batt_LF} + A \cdot \exp(-B \cdot it) \quad (1)$$

b) Charging ($I_{batt} < 0$)

$$V_{batt_i} = V_0 - k \frac{Q \cdot it}{Q - it} - k \frac{Q}{it + 0.1Q} I_{batt_LF} + A \cdot \exp(-B \cdot it) \quad (2)$$

where

$$it = \frac{1}{3600} \int_{t_0}^t I_{batt}(\tau) d\tau + Q \cdot (1 - SOC_{init}) \quad (3)$$

The explanation of variables in (1)–(3) is presented in Section III. In Fig. 4, the discharging curve of the implemented battery model is compared with the experimental data in [18].

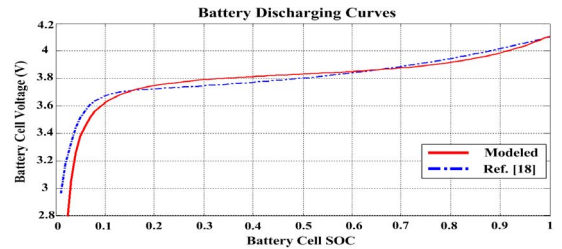


Fig. 4. Comparison between simulation result and experimental data

In Fig. 3, the DC-DC converter charges and discharges the PHEV battery by controlling the magnitude and direction of the current flowing through the converter. In this paper, the converter operates in buck mode when charging and in boost mode when discharging the battery, and it is implemented using the steady-state equations obtained from the topology in Fig. 3. Due to the internal resistance of the battery, overvoltage will occur before the battery is fully recharged if the charging current is not reduced. To prevent the overvoltage,

[20] applies the constant current and constant voltage (CC-CV) charging controller. In this paper, the way to determine I_{batt_ref} is slightly modified to consider the bidirectional time-varying current.

D. Inverter Current Controller and Current Distributor

The proposed building power system has upper-level controllers to distribute the total charging/discharging power reference to each PHEV based on its physical conditions and to control the input power of the building system in the case that none of the PHEVs are available for energy storage.

The Inverter Current Controller (ICC) adjusts the power flowing into or from the building system based on the states of the PHEV batteries. In detail, the ICC calculates the total current reference I_{tot_ref} for the batteries based on the power reference P_{comm} given from the grid operator and the output power of the rooftop PV generator. When all the voltage V_{batt} of the PHEV batteries increase to the maximum voltage V_{batt_max} and the amount of battery currents reduced by the CC-CV controller is not compensated by the natural reduction of the PV current, the ICC decreases the battery current reference I_{tot_ref} . Consequently, the inverter output current I_{inv} is reduced autonomously but slowly to allow grid-connected generators to change their output setting points without significant mechanical stress in a transient state. In this case, although there is a difference between the I_{inv} and the current reference I_{comm} calculated from the P_{comm} , the short-term fluctuation of the rooftop PV output and the high-frequency component of the power required for frequency regulation are still compensated by the batteries. As a result, the frequency deviation does not increase significantly. When the I_{comm} becomes equal to or smaller than the I_{inv} and the V_{batt} of at least one PHEV becomes lower than the V_{batt_max} with some margin, the ICC allows the building system input power to follow the P_{comm} again.

In addition, the Current Distributor (CD) enables the building system operator to assign different charging or discharging current reference to each PHEV. The reference is determined from the initial SOC SOC_{init} , desired charging end-time t_d , minimum SOC SOC_{min} , and V_{batt_max} under the constraint of power balance in the DC link. In this paper, the current ratio r_m for the PHEV_{*m*} is initially determined as

$$r_m = (1 - SOC_{init}^m) / t_d^m, \quad \text{for } m = 1, 2, \dots, N \quad (4)$$

where m is the index of the PHEV and N is the total number of the PHEVs participating in PV output power compensation and frequency regulation. The r_m determines the relative priority of the PHEVs in charging or discharging, and therefore, the desired and actual charging end-time of the batteries may be different because of unpredictable PV power. When the V_{batt} of PHEV_{*k*} increases to the V_{batt_max} , the CC-CV controller reduces its input current, and the CD then distributes the surplus current to other PHEVs_{*s*≠*k*} based on their initial current ratios $r_{j≠k}$.

When the SOC decreases to the SOC_{min} when discharging the PHEVs, the overall operations of the ICC and CD are similar, except that the CD decreases the corresponding r_m to 0 and that the ICC allows the PV current to flow to the AC grid when all the r_m become equal to 0. The complete operation sets of the ICC and CD are summarized in Tables II and III, where n is the number of the PHEVs available for energy storage (i.e., $V_{batt} < V_{batt_max}$ and $SOC > SOC_{min}$), and j and k are

TABLE II. OPERATION SET OF THE INVERTER CURRENT CONTROLLER (ICC)

Conditions	Inverter current (I_{inv})
A. $n > 0$	1. $I_{inv} = I_{comm}$
B. $n = 0$ (charging)	1. If $\Delta = 0$, then maintain I_{inv} as constant 2. Otherwise, decrease I_{inv} . 3. If $n \geq 1$ when I_{comm} decreases to $I_{inv} \pm \delta_I$, then $I_{inv} = I_{comm}$.
C. $n = 0$ (discharging)	1. $I_{inv} = -I_{PV_DC}$ 2. If $n \geq 1$ when I_{comm} increases positive, then $I_{inv} = I_{comm}$.

TABLE III. OPERATION SET OF THE CURRENT DISTRIBUTOR (CD)

Conditions	Battery current ratios (r_m)
D. $n = N$	1. Maintain all the r_j as constant.
E. $0 < n < N$	1. Charging: decrease r_k and increase r_j . 2. Discharging: decrease r_k to zero and increase r_j .
F. $n = 0$	1. Charging: maintain all the r_k as constant. 2. Discharging: maintain all the r_k at zero.

the indexes of the n and $(N-n)$ PHEVs, respectively. In addition, Δ is expressed by

$$\Delta = I_{inv} + I_{PV_DC} - \sum_{\text{all PHEVs}} I_{phev_DC} \quad (5)$$

and $\Delta = 0$ means that the PV current is so reduced that all the V_{batt} are maintained equal to or lower than the V_{batt_max} . For the operation presented in Table III, the CD is assumed to operate with programmable current limiters (PCLs), as shown in Fig. 5. Although there are several circuit models of the current limiters for battery charger application in [21] and [22], this paper considers them as current sources whose output is determined as the multiplication of the total charging/discharging current and corresponding PHEV current ratio.

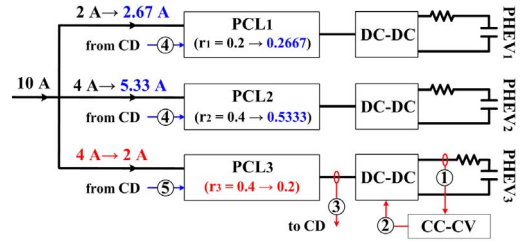


Fig. 5. Operating example of the programmable current limiters (PCLs)

E. Overall Building Power System

Fig. 6 presents a simplified configuration of the proposed building power system including the AC-DC bidirectional inverter, rooftop PV generator and multiple PHEVs. Each device has its own controller, and the power balance in the building system is maintained by the ICC and CD which are also implemented using SIMULINK blocks in order not to cause a significant increase in simulation time.

Specifically, Logic₁ in the ICC generates the Reset and SW_{sel} signals, which are active for B-3 or C-2 and C-1 in Table II, respectively. Furthermore, Logic₂ is implemented to prevent the undesirable fluctuation of the AC-DC inverter input power, which results from the PV power fluctuation, especially when all the V_{batt} are close to the V_{batt_max} . Therefore, as explained in B-3 in Table II, the I_{inv} changes to the I_{comm} for $|I_{comm} - I_{inv}| \leq \delta_I$, which is set to 2 A in this paper.

In the CD, the initial current ratio r_{im} is calculated using (4) beforehand, and the actual current ratio r_m is reduced by the PI_{CD} controller when the V_{batt} increases to the V_{batt_max} in charging or by the Block_{CD} when the SOC_m decreases to SOC_{min} in discharging. For other PHEVs still available for energy storage, the differential current ratio r_{dm} is determined by

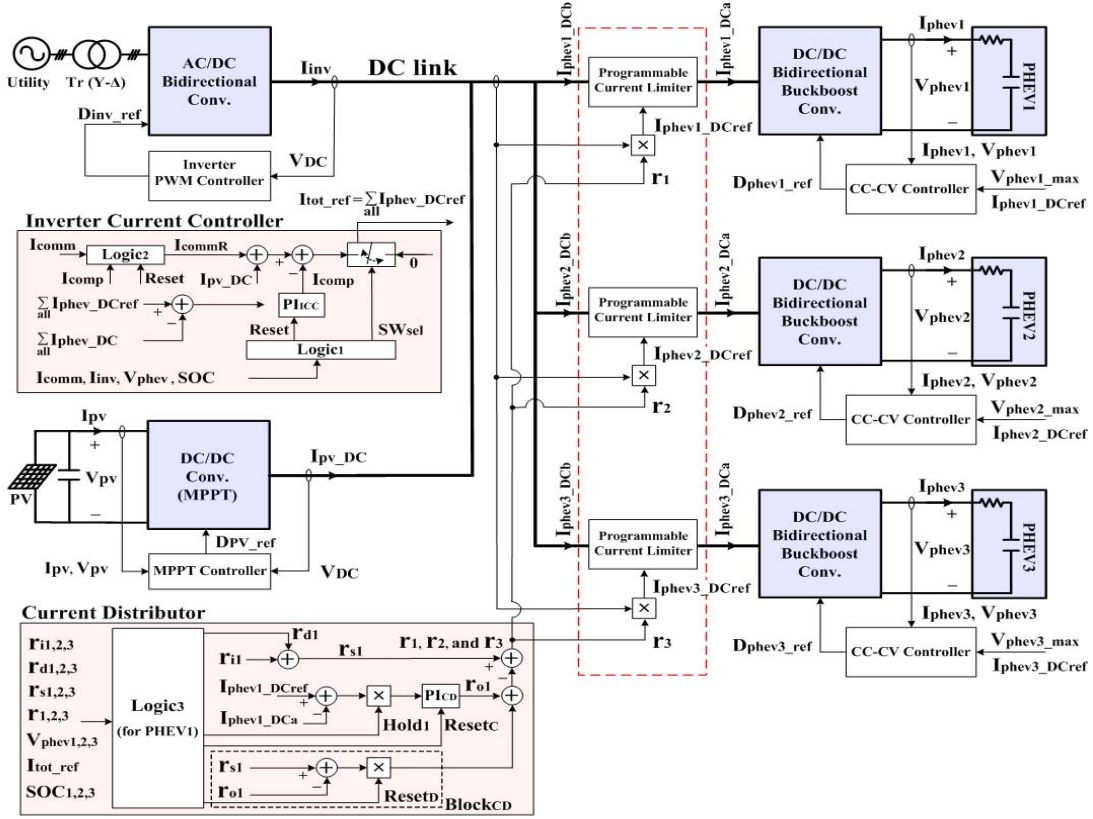


Fig. 6. Simplified configuration of the proposed building power system including the rooftop PV and multiple PHEVs

$$r_{dm} = r_m \sum_{q \in K} (r_{iq} - r_q) / \sum_{p \in J} r_p \quad \text{for } m \in J \quad (6)$$

where J and K are the set of the index j and k , respectively. This corresponds to E-1 and E-2 in Table III. The Reset_C is active when the PHEV owners change their current ratios r_m , and all the r_{dm} is set to 0 at the moment. The Hold_m and Reset_D signals are to fix the r_m as described by F-1 and F-2 in Table III, respectively.

III. CASE STUDIES AND RESULTS

A. Simulation Conditions

To analyze the proposed building system operation, time-domain simulation studies were performed under various conditions determined by: 1) the limitations of maximum voltage (Case 1) and minimum SOC (Case 3); 2) the rooftop PV output power fluctuation (Case 2); and 3) the frequency regulation signal (Case 4). The system specifications were determined based on the number and capacity of the PHEV batteries. For clear understanding, this paper considers three PHEVs as a representative case of the building with multiple PHEVs, and the corresponding specifications are presented in Table IV based on [19], [23], and [24] with slight modifications. Since the AC-DC inverter is modeled using per-unit values, its physical parameters can be easily modified according to the number of PHEVs. The SOC_{init} of the three PHEV batteries are 0.5, 0.65, and 0.35, respectively, and the corresponding r_m is initially determined as 0.5, 0.2, and 0.3, respectively. One-hour simulation results were obtained to verify the system operation in a reasonable time.

TABLE IV. DETAILED SPECIFICATIONS OF THE TEST SYSTEM

		AC-DC inverter
PV	Module	Inverter power rating (S_{inv_rated}): 40 kVA Nominal AC voltage (V_{phase}): 180 V ($V_{LL,rms} = 220$ V) Nominal AC frequency (f_{rated}): 60 Hz Rated DC link voltage (V_{DC_rated}): 600 V AC line resistance (R_{inv}): 0.0113 Ω AC line inductance (L_{inv}): 0.09 mH (Total line inductance from the PCCs to the inverter: 35 mH) DC link capacitance (C_{inv}): 4 mF DC link resistance (R_c): 0.01 Ω
	Array	Stabilized power (P_{PVm_rated}): 150 W Open circuit voltage (V_{ocr}): 43.4 V Voltage at peak power (V_p): 34.0 V Short circuit current (I_{scr}): 4.8 A Current at peak power (I_r): 4.4 A Dimensions: 1054 mm \times 1194 mm
PHEV battery		Battery rated capacity (Q): 16 kWh (47.06 Ah) Fully charged voltage (V_{full}): 395.76 V Nominal voltage (V_{nom}): 340 V Internal resistance (R_{bat}): 0.17225 Ω Battery constant voltage (V_0): 373.61 V Polarization constant (k): 0.0458 V/Ah or Ω Exponential zone amplitude (A): 25.67 V Exponential zone time constant (B): 0.1275 (Ah) ⁻¹

B. Case 1: Charging PHEVs with constant P_{comm} and $P_{PV} = 0$

In Case 1, the building system charges the PHEVs with constant power. Considering some voltage margin, the V_{phev_max} is set to 393 V, which can be differently assigned to each PHEV according to its desired final SOC. In Fig. 7, when the V_{phev1} increases to the V_{phev_max} at $t = t_1$, the PHEV₁ CC-CV controller decreases the I_{phev1} to prevent overvoltage. The CD and PCL then distribute the surplus current to the

PHEV₂ and PHEV₃ according to (6), as described by the increase in the $I_{phev,2,3}$ and $r_{2,3}$ for $t_1 \leq t \leq t_2$. It is similar to the PHEV charging profile in the period of $t_2 \leq t \leq t_3$ when the V_{phev2} also increases to the V_{phev_max} . When all the V_{phev} become equal to the V_{phev_max} at $t = t_3$, the r_m does not change further unless the PHEV owners decide to. All the I_{phev} are continuously reduced to 0 by the ICC as all the SOC increase close to 1.

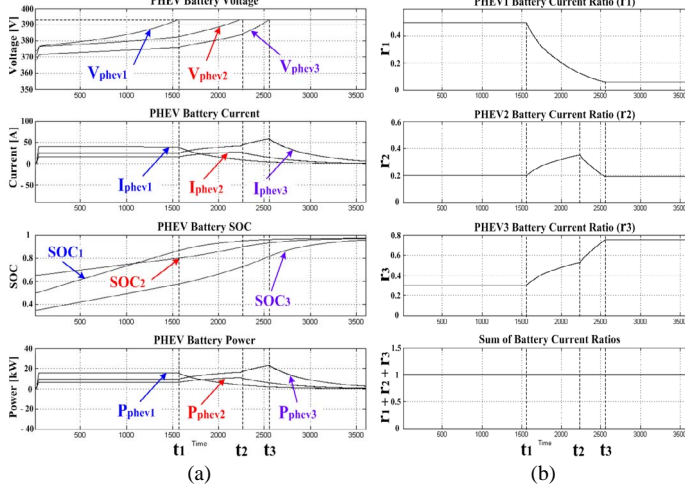


Fig. 7. Case 1: (a) the PHEV charging profiles and (b) current ratios

Fig. 8 shows that the I_{inv} is equal to the I_{comm} for $n \geq 1$. When the n decreases to 0 at $t = t_3$, the ICC gradually reduces the I_{inv} , regardless of the constant I_{comm} , for power balance in the building system. During the one-hour simulation period, the V_{DC} is regulated within $600 \text{ V} \pm 0.5\text{V}$.

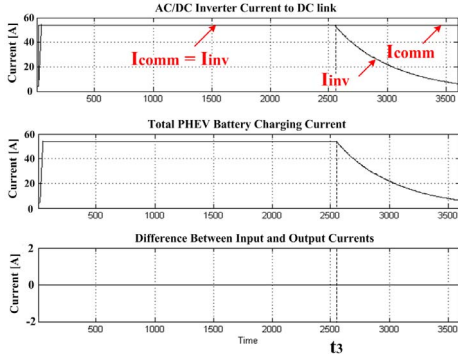


Fig. 8. Case 1: the inverter current, total PHEV current, and their difference

C. Case 2: Sequential changes in P_{comm} and unpredictable P_{pv}

To consider the effects of the rooftop PV array in Case 2, the solar insolation is assumed to be given with short- and long-term variation, as presented in Fig. 9(a), which is representative of a moderately cloudy day. The PV array voltage does not change significantly due to the intrinsic characteristics of the P_{PV} - V_{PV} curves, and therefore, the variation of the PV output power is similar to that of the insolation. In Case 2, the sequential step changes in the P_{comm} , and hence I_{comm} , are also considered as shown in Fig. 9(b). The I_{comm} varies from positive to negative for the analysis of the building system as a power load and source. In Fig. 9(b), the I_{inv} follows the I_{comm} for $0 \leq t \leq t_4$, when at least one PHEV is available for absorbing the PV power. For $t_4 \leq t \leq t_6$, the ICC reduces the I_{inv} but maintains it as constant when a decrease in the I_{PV} results in the reduction of the V_{phev} , which is consistent

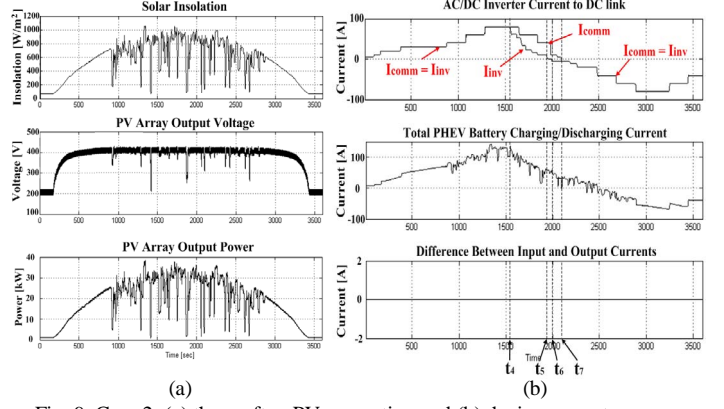


Fig. 9. Case 2: (a) the rooftop PV generation and (b) device currents

with B-1 in Table II. At $t = t_5$, the building system starts providing the grid or the internal load with power whose magnitude is determined based on the conditions of the PV and PHEVs. In addition, the I_{inv} follows the I_{comm} again at $t = t_7$ under the conditions explained in B-3 in Table II. Even during the period of $t_4 \leq t \leq t_7$ when there is the current deviation between the I_{inv} and I_{comm} , the rapidly fluctuating component of PV power is still compensated for by all the PHEVs. The slow and smooth change of the I_{inv} can be properly compensated for by generators regulating the grid frequency. Fig. 10 presents the simulation results of the PHEV charging/discharging profiles. The PV short-term fluctuation is reflected on the I_{phev} , and consequently V_{phev} , but its effect on SOC swing is negligible.

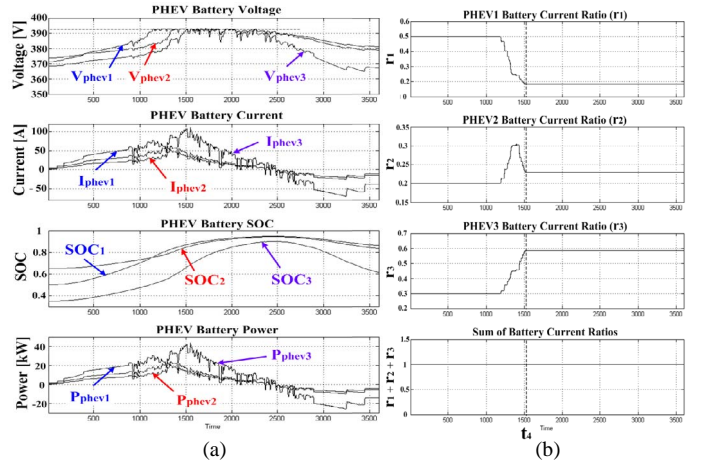


Fig. 10. Case 2: (a) the PHEV charging profiles and (b) current ratios

D. Case 3: Discharging PHEVs to SOC_{min}

In Case 3, all the PHEV batteries are discharged to SOC_{min} . The PV output power is scaled down by a factor of 0.4. In Fig. 11, when the SOC_3 decreases to the SOC_{min} at $t = t_8$, the CD almost immediately reduces the $|I_{phev3}|$ to 0, and distributes the insufficient discharging current to the PHEV₁ and PHEV₂, as described by the increase in the $|I_{phev1,2}|$. It is repeated until $t = t_{10}$ when all the SOC become equal to the SOC_{min} . For $t_{10} \leq t \leq t_{11}$, all the PHEVs are in an idle state, and the ICC allows the rooftop PV current to flow to the AC grid through the AC-DC inverter, as explained in C-1 in Table II. It is equivalent to a conventional operating method of the grid-connected rooftop PV generator. At $t = t_{11}$ when the I_{comm} changes to positive, the batteries start being charged and then become available for energy storage again, which enables the

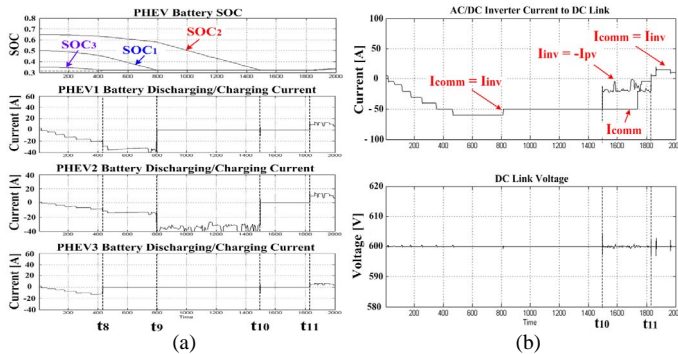


Fig. 11. Case 3: (a) the PHEV charging profiles and (b) the inverter current (top) and DC link voltage (bottom)

I_{inv} to follow the I_{comm} . At $t = t_{11}$, the current ratios r_m for all m were reassigned according to PHEV owners' decisions.

E. Case 4: Adding frequency regulation power (P_{reg}) to P_{comm}

In Case 4, it is simply assumed that a number of the proposed building power systems are connected to the AC grid. They participate in frequency regulation by compensating for the high-frequency component of the load frequency control signal. The conventional thermal and hydro generators are responsible for the remaining component of the signal. The utility operator then determines the power required for compensating for the high-frequency signal and adds it to the AC-DC inverter input power reference.

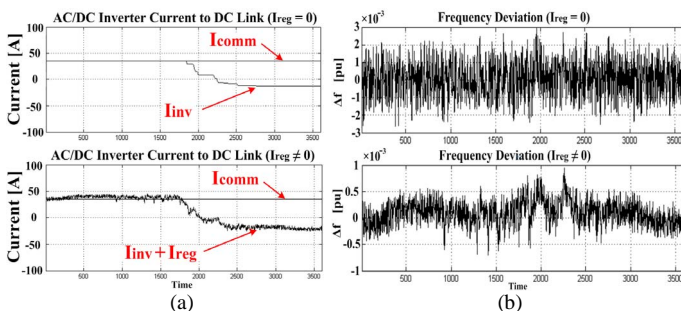


Fig. 12. Case 4: (a) the inverter current and (b) system frequency for the $I_{reg} = 0$ (top) and $I_{reg} \neq 0$ (bottom)

Fig. 12 compares the simulation results of the inverter current and grid frequency according to whether or not the proposed building systems participate in the frequency regulation. In both cases, they still compensate for the rooftop PV output. Fig. 12 shows that, with a given time-varying load demand, the frequency deviation is reduced to less than 34 % when the building systems coordinate with the conventional generators in the grid. All the SOC of the PHEVs are not significantly affected by the regulation current I_{reg} because its long-term average is close to 0.

IV. CONCLUSION

This paper presents an alternative system for a commercial building with a rooftop PV generator and multiple PHEVs. The objective of the proposed building system is to compensate for the rooftop PV output fluctuation by charging/discharging multiple PHEVs with different amounts of power under various conditions such as initial SOC level and the limitations of maximum battery voltage and minimum SOC. The proposed system was designed and implemented using steady-state and dynamic models of power electronic devices

as well as controllers at device and system levels. The simulation results demonstrate that the proposed system performed as intended, enabling the grid operator to consider the building an important aggregator for frequency regulation.

REFERENCES

- [1] R. Yan and T. K. Saha, "Investigation of voltage stability for residential customers due to high photovoltaic penetrations," *IEEE Trans. Power Syst.*, vol. 27, no. 2, pp. 651-662, May 2012.
- [2] I. Cvetkovic, "Modeling, analysis and design of renewable energy nanogrid systems" M.S. thesis, Dept. of Elect. Eng., Virginia Polytechnic Institute and State Univ., Virginia, USA, July 2010
- [3] E. Navarro, "International standard situation concerning components of distributed power systems and recommendations of supplements," Dispower Project Report (Del_2005_0070), Sep. 2005
- [4] Y. J. Kim, S. J. Ahn, P. I. Hwang, G. C. Pyo, and S. I. Moon, "Coordinated control of a DG and voltage control devices using a dynamic programming algorithm," *IEEE Trans. Power Syst.*, Early Access, 2012.
- [5] M. Coddington *et al.*, "Photovoltaic systems interconnected onto secondary network distribution systems—Success stories," National Renewable Energy Laboratory Technical Report (NREL/TP-550-45061), April 2009.
- [6] K. Garbesi, V. Vossos, A. Sanstad, and G. Burch, "Optimizing energy savings from direct-DC in U.S. residential buildings", Direct-DC Power Systems Project (LBNL-5193E), Oct. 2011
- [7] M. D. Galus, S. Koch, and G. Andersson, "Provision of load frequency control by PHEVs, controllable loads, and a cogeneration unit," *IEEE Trans. Ind. Electron.*, vol. 58, no. 10, pp. 4568-4582, Oct. 2011.
- [8] R. Hara *et al.*, "Testing the technologies," *IEEE Power Energy Mag.*, vol. 7, no. 3, pp. 77-85, 2009.
- [9] T. Markel, K. Smith, and A. Pesaran, "PHEV energy storage performance/life/cost trade-off analysis," in *Proc. 8th Advanced Automotive Battery Conf.*, May. 2009.
- [10] T. Masuta and A. Yokoyama, "Supplementary load frequency control by use of a number of both electric vehicles and heat pump water heaters," *IEEE Trans. Smart Grid*, vol. 3, no. 3, pp. 1253-1262, Sep. 2012.
- [11] P. Denholm and R. M. Margolis, "Impacts of array configuration on land-use requirements for large-scale photovoltaic deployment in the United States," in *Proc. American Solar Energy Society Conf.*, May 2008.
- [12] K. Garbesi *et al.*, "Catalog of DC appliances and power systems," Direct-DC Power Systems Project (LBNL-5364E), Oct. 2011
- [13] L. Dickerman and J. Harrison, "A new car, a new grid," *IEEE Power Energy Mag.*, vol. 8, no. 2, pp. 55-61, 2010.
- [14] Wolf, K. L. "Trees, parking and green law: strategies for sustainability," Georgia Forestry Commission, Urban and Community Forestry, 2004.
- [15] Y. J. Kim, P. Hwang, S. Moon, "A steady-state analysis for an inverter-based DG to determine the optimal capacity of an inverter and harmonic filters," *J. Int. Council Elect. Eng.*, vol. 1, no. 1, pp. 14-20, Jan. 2011.
- [16] M. G. Villalva, J. R. Gazoli, and E. R. Filho, "Comprehensive approach to modeling and simulation of photovoltaic arrays," *IEEE Trans. Power Electron.*, vol. 24, no. 5, pp. 1198-1208, May 2009.
- [17] M. Datta *et al.*, "A frequency-control approach by photovoltaic generator in a PV-diesel hybrid power system," *IEEE Trans. Energy Convers.*, vol. 26, no. 2, pp. 559-571, June 2012.
- [18] M. Chen and G. A. Rincon-Mora, "Accurate electrical battery model capable of predicting runtime and I-V performance," *IEEE Trans. Energy Convers.*, vol. 21, no. 2, pp. 504-511, June 2006.
- [19] O. Tremblay, L. A. Dessaint, and A. I. Dekkiche, "A generic battery model for the dynamic simulation of hybrid electric vehicles," in *Proc. Vehicle Power and Propulsion Conf.*, Sep. 2008.
- [20] K. Morrow, D. Karner, and J. Francfort, "Plug-in hybrid electric vehicle charging infrastructure review," US DOE Technologies Program: Advanced Vehicle Testing Activity (INL/EXT-08-15058), Nov. 2008.
- [21] Linear Technology LTC4000 High Voltage High Current Controller for Battery Charging and Power Management, [Online]. Available: www.linear.com/docs/39757, Linear Technology.
- [22] Hybrid and Electric Vehicle Solutions Guide, [Online]. Available www.ti.com/lit/ml/szza058a/szza058a.pdf, Texas Instrument.
- [23] A. H. Fanney, K. R. Henderson, and E. R. Weise, "Measured performance of a 35 kilowatt roof top photovoltaic system," in *Proc. Int. Solar Energy Conf.*, May 2003.
- [24] K. P. Louganski, "Modeling and analysis of a DC power distribution system in 21st century airlifters" M.S. thesis, Dept. of Elect. Eng., Virginia Polytechnic Institute and State Univ., Virginia, USA, Sep. 1999.